Supplementary Materials: Cloud shadows drive vertical migrations of deep-dwelling marine life

Melissa M. Omand*[1], Deborah K. Steinberg[2], Karen Stamieszkin[2]
*corresponding author: momand@uri.edu
[1] Graduate School of Oceanography, University of Rhode Island
[2] Biological Sciences Dept., Virginia Institute of Marine Science (VIMS)

Data were collected from the *R/V Revelle* during the 2018 EXPORTS field campaign (Siegel et al. 2021) in August and September near Ocean Station Papa (145°W, 50°N) (gray lines, Fig. S1). A Wirewalker (WW), a drifting wave-powered profiling platform was deployed for 23 days, obtaining 564 profiles. The Wirewalker consisted of a surface buoy with a 500 m wire hanging vertically beneath it and a clump weight at the bottom. A profiling platform was clipped onto the wire, and equipped with various instruments, of which the CTD (RBR Maestro), chlorophyll fluorescence and optical backscatter sensors (WetLabs ECOtriplet), and a photosynthetically active radiation sensor PAR_z (JFE Advantech DEFI-L) are used in this analysis. The Wirewalker platform is propelled down the wire with a one-way ratcheting mechanism. At the bottom, the mechanism is released and the Wirewalker glides to the top of the wire, and repeats. Over the course of the cruise, the Wirewalker was repositioned three times at roughly 8 day intervals, near a Lagrangian float (red lines, Fig. S1). The *R/V Revelle* followed the drifting assets, generally staying within 4 km (grey lines, Fig S1). In addition to the aforementioned WW data, this study utilizes two data types from the ship: 1) surface Photosynthetically Active Radiation (PAR_o, Biospherical QSR-2200, see Fig S2a) and 2) acoustic backscatter intensity (AB) from the hull-mounted narrowband 150 kHz Acoustic Doppler Current Profiler (ADCP, RD Instruments, see Fig S2b).

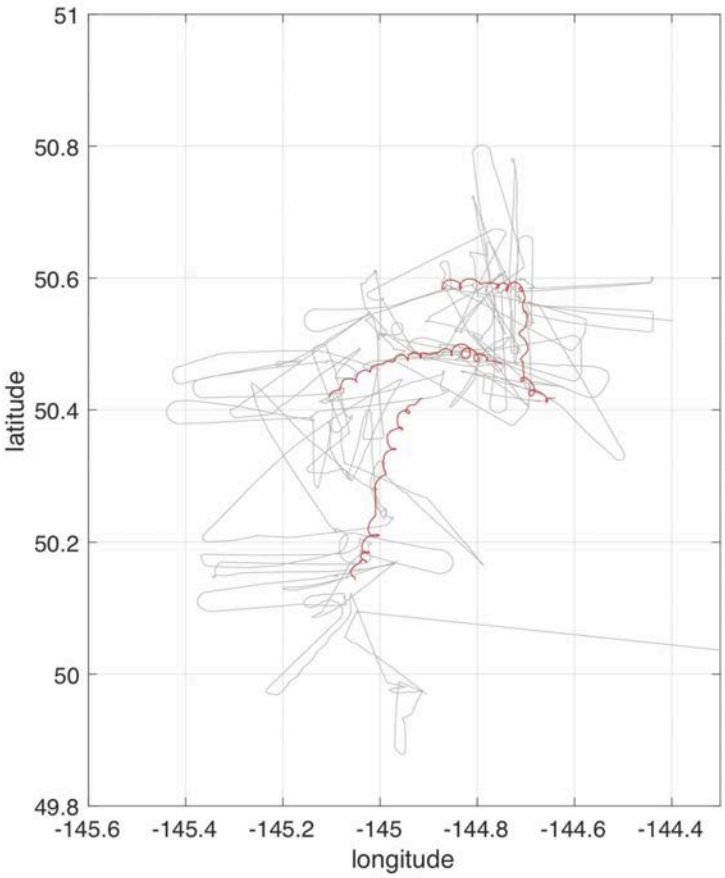

Figure S1: *Tracks of the R/V Revelle (gray) and the drifting Wirewalker (red) during the 2018 EXPORTS cruise near Ocean Station Papa in the subarctic North Pacific Ocean.*

In post-cruise data processing, we found that the PAR_o sensor on the *R/V Revelle* was biased high, and saturated at 4265 $\mu Em^{-2}s^{-1}$ whereas all other PAR_o measurements (from the WW buoy, the PMEL mooring, and a nearby vessel R/V *Sally Ride*) showed a maximum of about 2000 $\mu Em^{-2}s^{-1}$. The *Revelle* PAR_o was highly correlated with the WW buoy PAR_o and was corrected with a linear fit (slope = 0.300, intercept = 11.5 $\mu Em^{-2}s^{-1}$). Thus, PAR_o used for this analysis saturates at 1280 $\mu Em^{-2}s^{-1}$ (Fig. 1a), however, since the saturation occurs in only 0.3% of the measurements, it does not adversely affect our results. After intercalibration of the ship's PAR_o sensor, the 15-second PAR_o data was interpolated onto the 2 minute ADCP interval and smoothed with a 5 point filter for all except the analysis shown in Fig S6.

Raw acoustic backscatter (AB) from the duration of the cruise (Fig. S2b) exhibited decreasing amplitude with depth typical of hull-mounted sensors, and a clear pattern of diel vertical migration. Persistent migrating layers were observed to descend maximum depths of approximately 50 m, 150 m, and 300m around noon. Other layers also occurred, but were more ephemeral. Of these, the deepest layer (reaching 300 m) was the most distinct, with a very tight and well-defined vertical distribution (Fig. S2c).

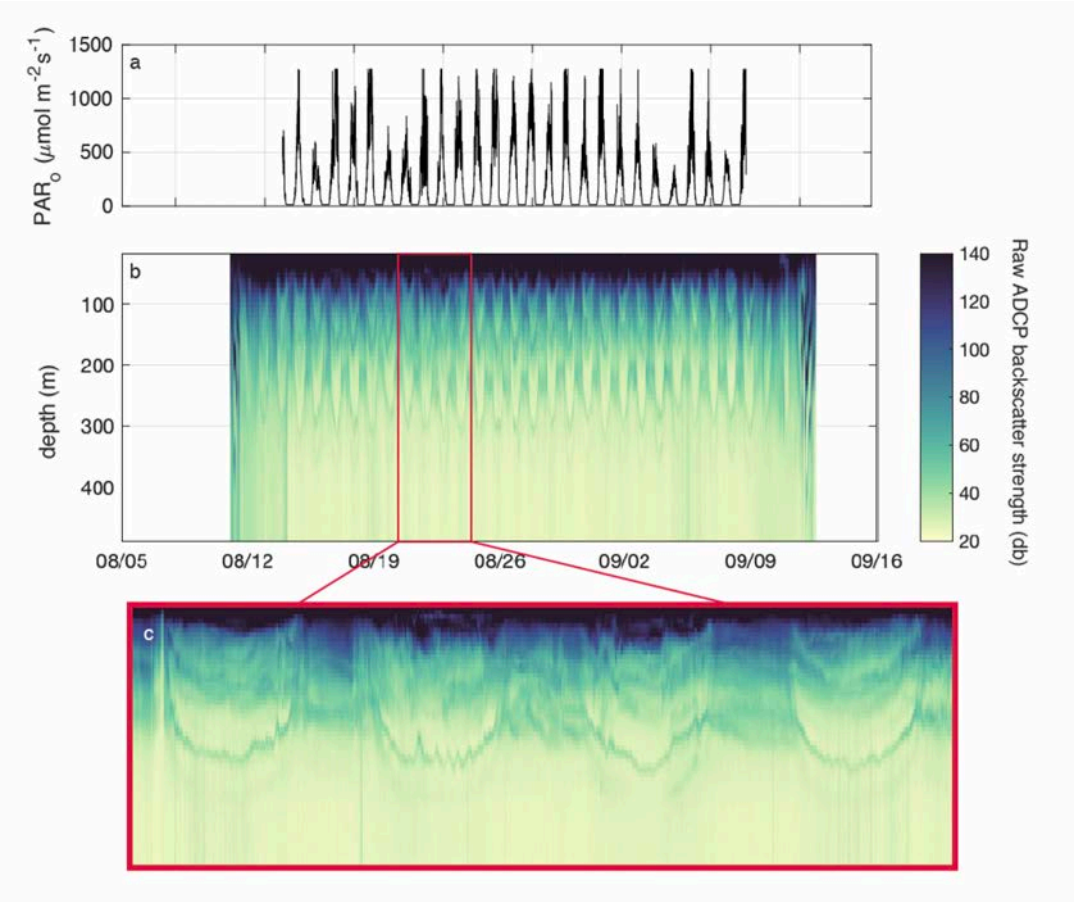

Figure S2: *The entire 26-day time-series of a) surface incident PAR, and b) raw acoustic backscatter (AB) from the hull-mounted ADCP. A zoomed in segment of threw data is shown in panel c. Various scattering layers were evident in the raw time-series, with the layer reaching 300m showing the most distinct distribution and strongest evidence of high frequency migrations.*

High resolution observations of near surface light profiles:
Below the surface, a profile of PAR_z was obtained from the Wirewalker (WW) roughly every 40 minutes. The noise floor of this sensor is 1 $\mu Em^{-2}s^{-1}$, and thus data below this value were removed (white spaces, Fig. 1b), providing measurements of PAR that resolved diel and cloud-driven variations down to 85 m depth during high noon. A euphotic zone diffuse attenuation coefficient (k_{eu}) of 0.065 m^{-1} was calculated from a linear fit (in log space) to the average of 37 PAR_z WW profiles collected between 10:00 and 14:00 local time (grey points, Fig 1c). To evaluate temporal variability in k_{eu}, fits were also performed for each profile, yielding a standard deviation of 0.004 m^{-1}. The euphotic depth (z_{eu}), defined as the 1% light level, was determined from k_{eu} according to

$$z_{eu} = -ln(0.01)/k_{eu} \quad (3)$$

The average euphotic depth of 71 m coincided with the base of the deep Chl-a fluorescence (blue line, Fig. 1c) and optical backscatter (red line, Fig. 1c) maximum.

Modeling of the light field in the twilight zone:
PAR_{mod} below the euphotic depth (the upper twilight zone) (between 71 and 350 m) was modeled using a diffuse attenuation coefficient of k_{tz} = 0.03 m^{-1} (Fig. 1c) according to

$$PAR_{mod} = PAR(z = 71m)e^{k_{tz}z} \quad (4)$$

The value for k_{tz} was determined recursively through scaling the amplitude of the observed variations in the DSL (black line, Fig. 1e) to match the amplitude of the modeled isolume contours (white contours, Fig. 1d,e). Numerous factors can contribute to uncertainties in the effort of modeling twilight zone light. Variations in inherent optical properties, often driven by

phytoplankton or sediments, can alter the attenuation of light and produce a deep migratory response[2]. Surface Waves can impact light underwater through wave focusing[3] and surface roughness due to wind and waves can influence the amount, and spectral distribution of light that penetrates the air-sea interface[4]. Darkening of the twilight zone can occur due to a reduction in incident sun and an increase in light scattering due to rain and waves. Kaartvedt et al. (2017)[5] documented the mesopelagic response to a passing rain storm in the Red Sea that extended even to DSLs at 600m depth. They find diffuse attenuation coefficients of the euphotic and and twilight zones 0.063 ± 0.001 m^{-1} and 0.038 ± 0.002 m^{-1} respectively, that are very similar to our values of 0.065 m^{-1} and 0.030 m^{-1}.

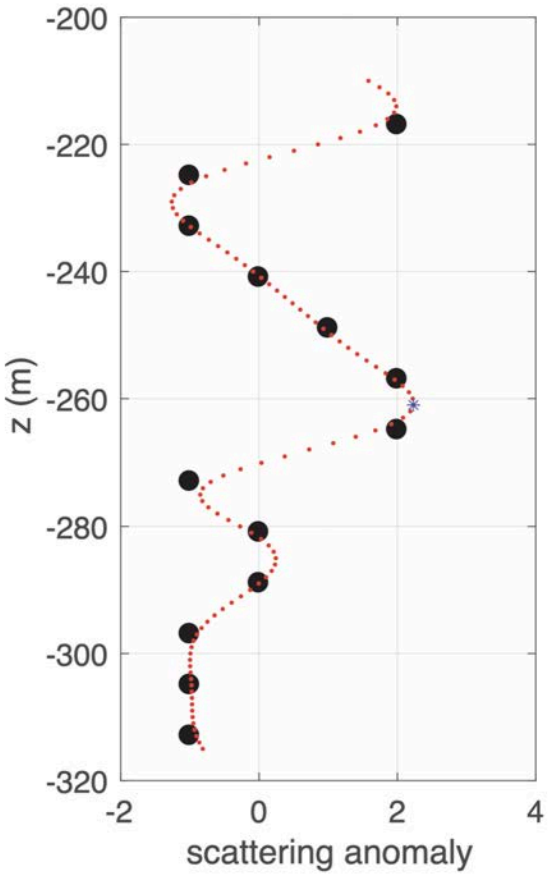

Figure S3: *An example of a single profile of AB' with the original 8 m bins (black points) and the objectively mapped estimates at 1 m resolution (red points). The DSL was detected by finding the maximum in the objectively mapped AB', indicated by the blue asterisk.*

Objective mapping of the acoustic backscatter:

The acoustic backscatter from the 150 KHz Acoustic Doppler Current Profiler (ADCP) was processed according to standard CODAS methods and binned into 2 minute intervals. Data were collected with vertical bin spacing was 8 m; no averaging was done in the vertical[6]. Anomalies in the acoustic backscatter (*AB'*) were calculated by subtracting the signal at each depth from the time-averaged backscatter at that depth, according to:

$$AB'(z,t) = AB(z,t) - < AB(z) > . \quad (5)$$

Multiple scattering layers were evident between 100 and 400m depth during the day, and many showed a correspondence between the cloud-driven isolume variations and the layer depths. The DSL occurring at approximately 280 m at high noon was especially thin, with a strong scattering signal, and thus was selected for the more detailed analysis described here. To isolate this layer, we used a technique called objective mapping[7]. This method can be applied to sparse datasets to enable estimation of the information between the measurements. Here, the 8 m binned AB' data was objectively mapped onto a 1 m vertical grid between 210 and 320 m, using a vertical decorrelation scale of 7 m and a noise to signal ratio of 0.2. An example of an objectively mapped profile is shown in Fig. S3. This example demonstrates that the autocorrelation in these profiles can be used to refine our estimate of the depth of the local maxima in AB' (blue star). This proved to be a crucial step in extracting the correlations between the DSL and PAR (shown in Fig. 2), where variations of the layer (or isolumes) were often only ~10m - a similar scale to the initial 8m bin size of the ADCP.
The DSL was determined by selecting the maximum in each objectively mapped AB' profile between 210 and 320 m depth. Once completed, the DSL was manually inspected for outliers - situations where the maximum had abruptly jumped from the main peak to a secondary one (for example, see the secondary peak near z = -218 m in Fig. S3). Out of 18720 profiles, this occurred in only 26. These points were excluded from the analysis. A comparison between the DSL that would be obtained from the 8m bins (black line, Fig. S4a) and the mapped data (black line, Fig. S4b) demonstrates the fine detail that can be extracted due to the autocorrelation of information in the more coarsely gridded observations.

Calculation of the correlation coefficients and significance

The correlations shown in Fig 3a were calculated for each day (during daylight hours) between the high-pass filtered PAR (subsampled to match the 2 minute interval of the ADCP) and the high-pass filtered layer depth. The correlation coefficient (r^2) and the p-value were computed using the MatLab function corrcoef.m modified to exclude NaNs from the correlation and the degrees of freedom (number of independent data points). Since each 2 minute interval represents an independent mea-

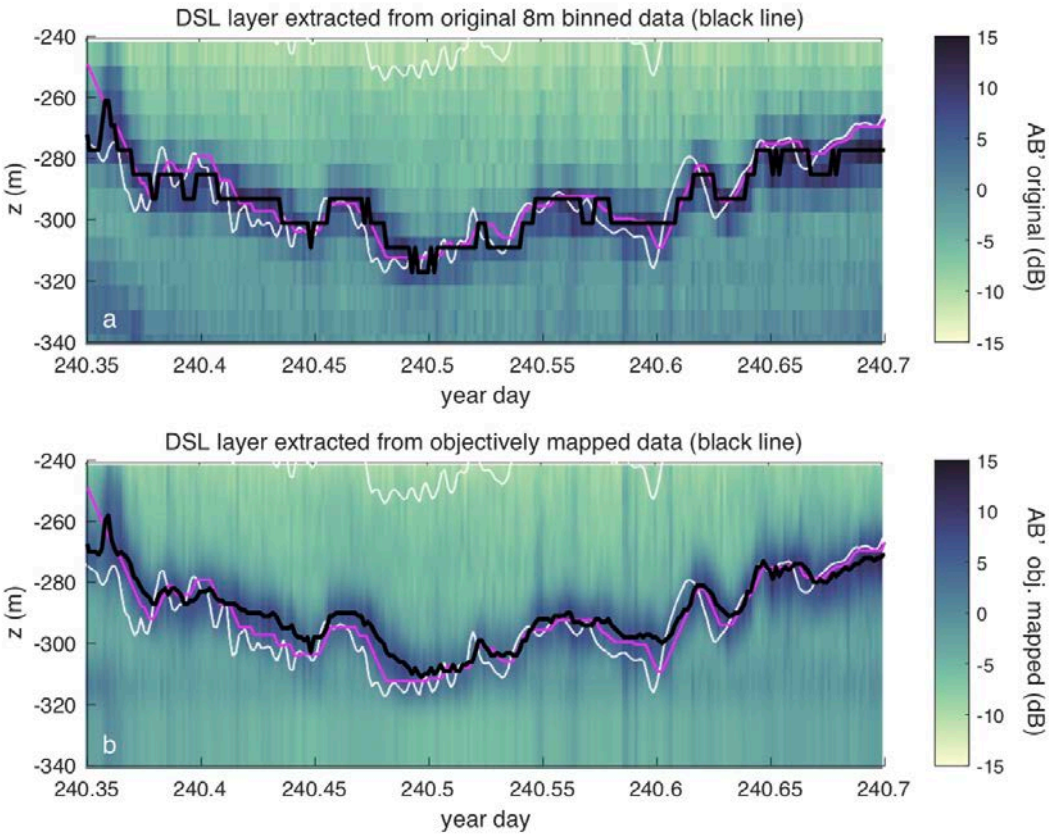

Figure S4: *An 8-h example of acoustic backscatter anomaly (AB') from a) the original 8m binned data, and b) the objectively mapped 1m data. The black line indicates the DSL determined from the AB' maximum between 210 and 320m for the original and objectively mapped cases. White lines indicate the contours of PAR (white lines). In b), the correlation between the DSL (black) and the phototactic swimming model (magenta, assessed solely from PAR) demonstrates that detailed information on scattering layers can be extracted from coarsely-binned ADCP records.*

surements, all data points were included in the significance calculation. We used the stringent criteria of $p<0.001$ to determine when the correlation is significant, meaning that there is a 0.001 probability of getting a correlation as large as the observed value by random chance.

Organisms that compose the DSL:

Zooplankton and micronekton biomass and taxonomic composition were determined within nine discrete depth intervals between 0-1000m using a 1 m^2, 200 µm mesh MOCNESS (Multiple Opening/Closing Net and Environmental Sensing System). The HFM DSL analyzed herein was located at 280m, near the boundary of the peak daytime biomass peak (300-400m) as sampled by the net; the increase in biomass in the upper 0-100m surface layers due to DVM can be seen at night (Fig. S5a). The DVM community was dominated by >2 mm animals (Fig. S5a), which included crustaceans (Fig. S7b-d) and gelatinous (Fig. S5e) forms which can be seen migrating from various depths in the twilight zone during the day into the surface 150m at night.

The rate of change hypothesis:

The rate of change hypothesis states that vertical migration is initiated by the relative rate and direction of changing light intensity. This hypothesis is supported by laboratory studies that quantify photoresponse thresholds (the amount of relative change in ambient light required to produce a migratory response) for various zooplankton species (red dashed lines, Fig. S6). These thresholds are close to the reported typical rates of change observed at dawn and dusk (blue dashed lines, Fig. S6), and Cohen and Forward (2009)[8] hypothesize that this allows avoidance of a migratory response due to clouds (that are presumed to produce smaller relative rates of change). Here, we quantify the relative rate of change of the ambient PAR at 380m - the average daytime DSL depth - following [8]. The relative rate of change in light intensity (RR) - the first derivative of the ambient PAR (PAR_{380m}) - is computed with respect to time (at 2 min intervals), and then normalized by the magnitude:

$$\mathrm{RR} = (PAR_{380m})^{-1} dPAR_{380m}/dt \qquad (6)$$

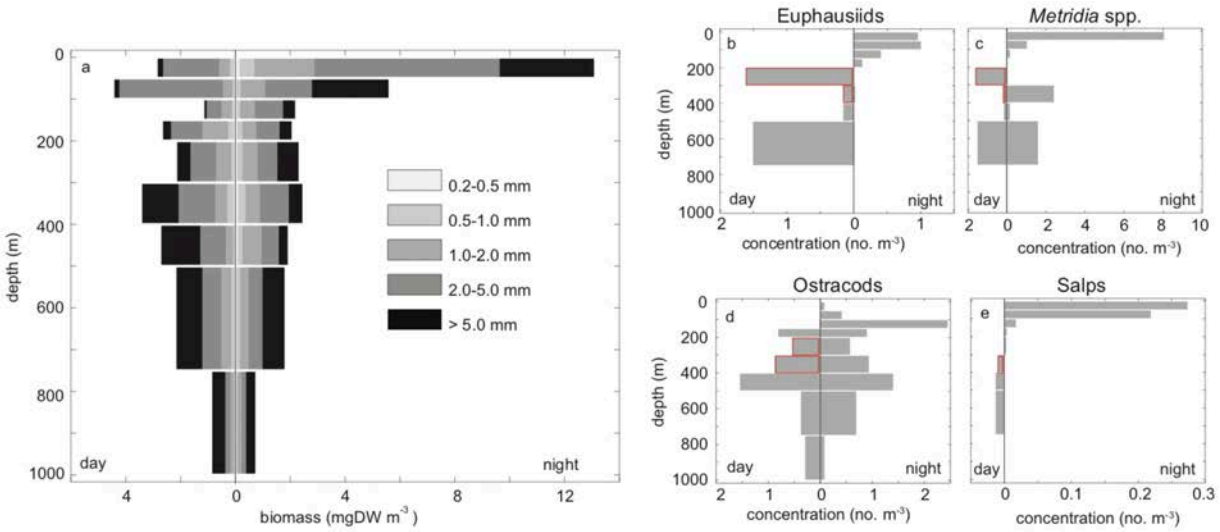

Figure S5: *a) Mean day and night zooplankton biomass, divided by five size fractions (0.2-0.5, 0.5-1.0, 1.0-2.0, 2.0-5.0, > 5.0 mm; [8]), over nine depth strata between 1000 m and the surface. Values are the average of six day/night pairs of MOCNESS tows, and panels b)-e) Day and night abundance of strongly migrating zooplankton, including crustacean (euphausiids, the calanoid copepod Metridia spp., and ostracods) and gelatinous (salps) taxa. The daytime depth strata that straddle the DSL analyzed here is outlined with red.*

Dawn and dusk were defined as periods with surface PAR_o less than 30 $\mu Em^{-2}s^{-1}$ (with points less than the noise threshold of 1 $\mu Em^{-2}s^{-1}$ excluded). Daytime was defined where surface PAR_o was greater than 30 $\mu Em^{-2}s^{-1}$, constituting 92% of our measurements (9963 of 10801). We observed a maximum dawn/dusk relative rate of change (blue bars) of ~0.003 s^{-1} consistent with many of the previously reported maximum values. However, we also find that the cloud-driven rates of change (white bars) are well within, and often exceed, the rates observed during sunrise and sunset. These rates range from near zero up to a maximum of about 0.006 s^{-1}. Our analysis suggests that cloud-driven PAR variations are often sufficiently large but within the range of detectability, to produce a migratory photoresponse by the zooplankton species listed in Fig. S5.

Evaluating the contributions of internal waves to DSL depth:
Internal waves have amplitudes that are comparable to the size of the high frequency DSL migrations. The super-inertial variability in deep isopycnals measured by the pseudo-Lagrangian Wirewalker platform (Fig. S7) is dominated by internal waves[23]. It is clear from comparing the excursion distances of the isopycnals (white contours) with the DSL depth (black lines) that the vertical motion of the isopycnals are likely to impose velocities that must be overcome in order to maintain isolume-tracking. The variability imposed onto the DSL due to vertical advection was quantified from the amplitude of isopycnal excursions (A_{iso}) according to

$$A_{iso} = | z_{iso} - \overline{z_{iso}} | \qquad (7)$$

where z_{iso} is the isopycnal depth (white contours, Fig. S7), the overbar indicates a time average, and the vertical bars indicate an absolute value. The histogram of A_{iso} is shown in Fig. S8a, indicating a range in amplitude up to 24.6 m and a standard deviation of 7.4 m. This distribution can be compared with that obtained from the same analysis applied to the high-pass DSL anomalies (Fig. S8b). We find that both encompass the same range, with DSL' reaching a maximum of 41.5 m, but having a slightly lower standard deviation of 5.8 m. These results demonstrate that in the absence of swimming, internal waves would have a significant effect on the depth of the DSL, producing variations in depth comparable to those observed. However, if the organisms were passively vertically advected on isopycnals, we would not see the strong correspondence between their depth and the isolumes. This leads us to conclude that the migrators are swimming sufficiently to overcome both cloud-driven variations, and internal oscillations of density surfaces.

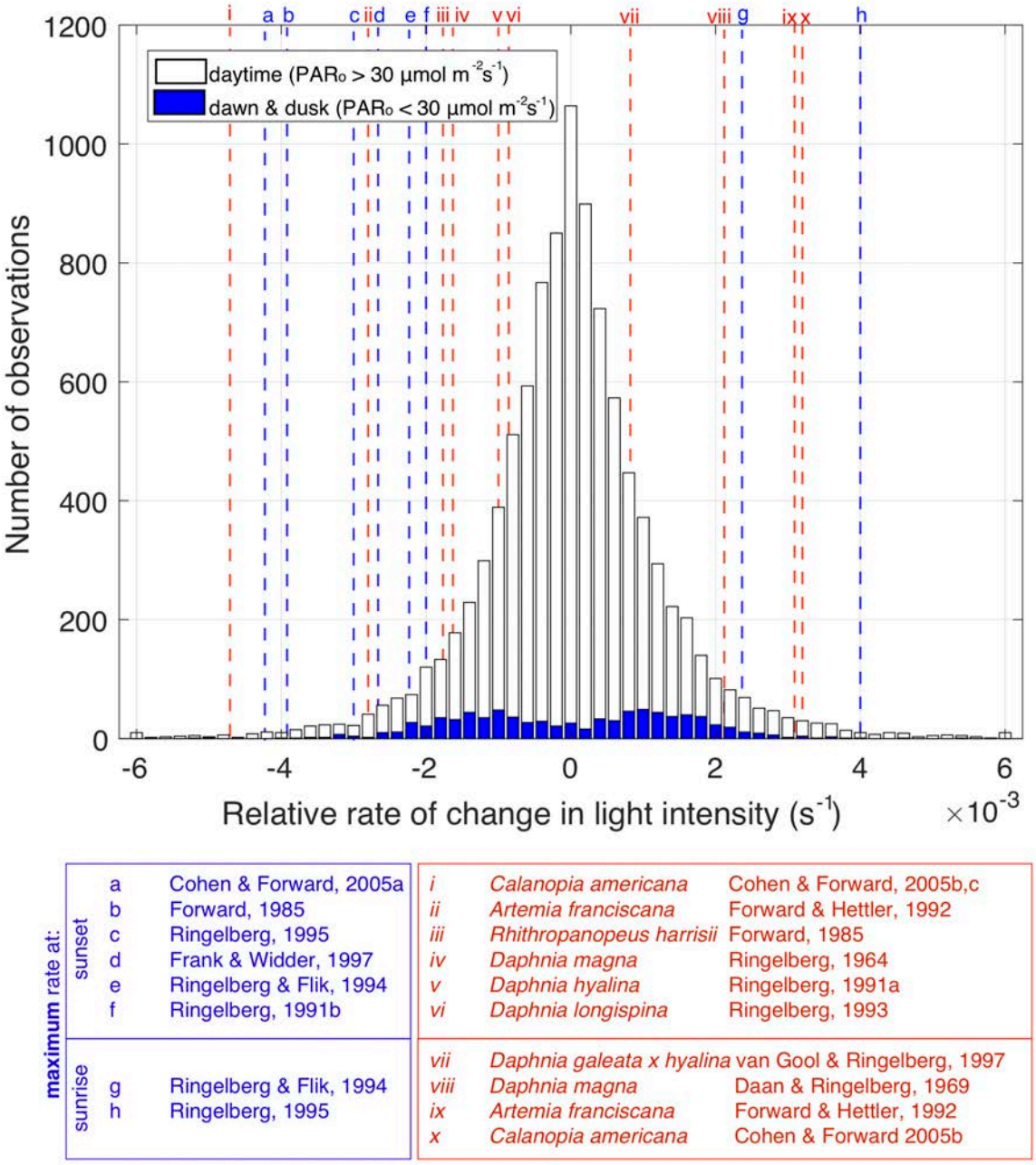

Figure S6: *A histogram of the relative rate of change in the ambient light at 280m (the average DSL daytime depth) due to cloud-driven oscillations during the day (white bars, defined as $PAR_o > 30\ \mu Em^{-2}s^{-1}$), and during dawn and dusk (blue bars, defined as $PAR_o < 30\ \mu Em^{-2}s^{-1}$). Vertical blue dashed lines indicate the maximum relative rate of change at dawn and dusk, and red dashed lines indicate the thresholds for photoresponses for zooplankton species, as compiled by Cohen and Forward (2009).*

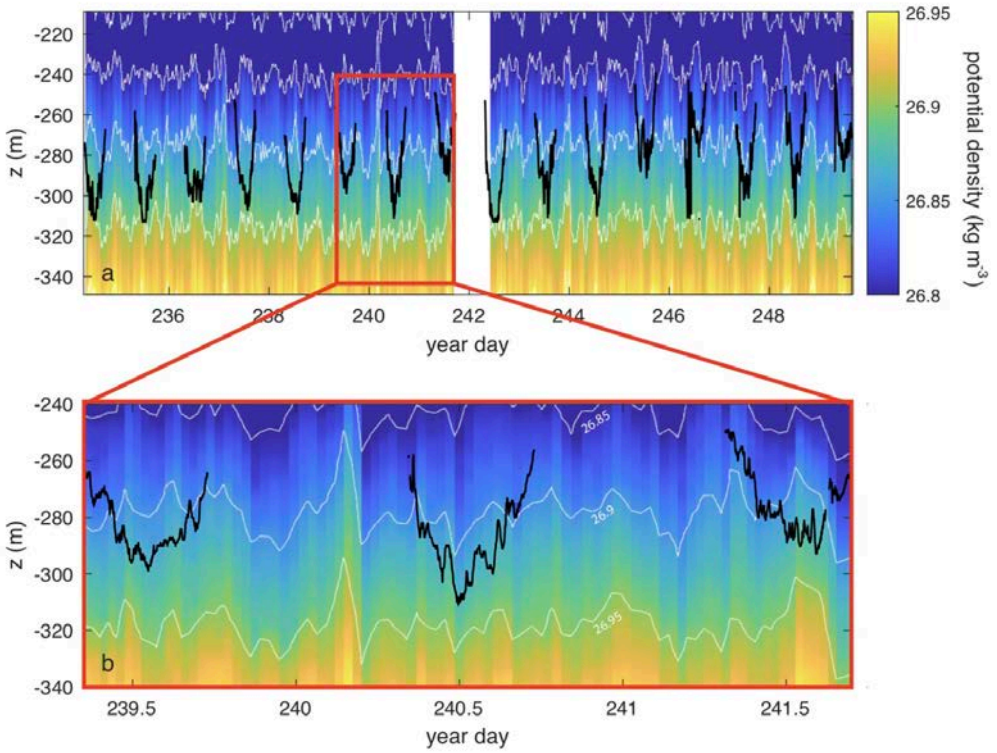

Figure S7: *a) A 16 day record, and b) a 2.4 day inset, of 40 minute profiles of potential density from the Wirewalker (colors), with isopycnal depths shown as white contours (0.05 kg m^{-3} intervals). The Deep Scattering Layer (DSL) is shown with the black line, demonstrating that the internal wave-driven isopycnal excursions have a similar magnitude to the high frequency DSL migrations. Even so, we show that the DSL variations are not generated by the internal waves. Instead, the migrators must be swimming against the internal wave-induced vertical velocity in order to maintain isolume-tracking.*

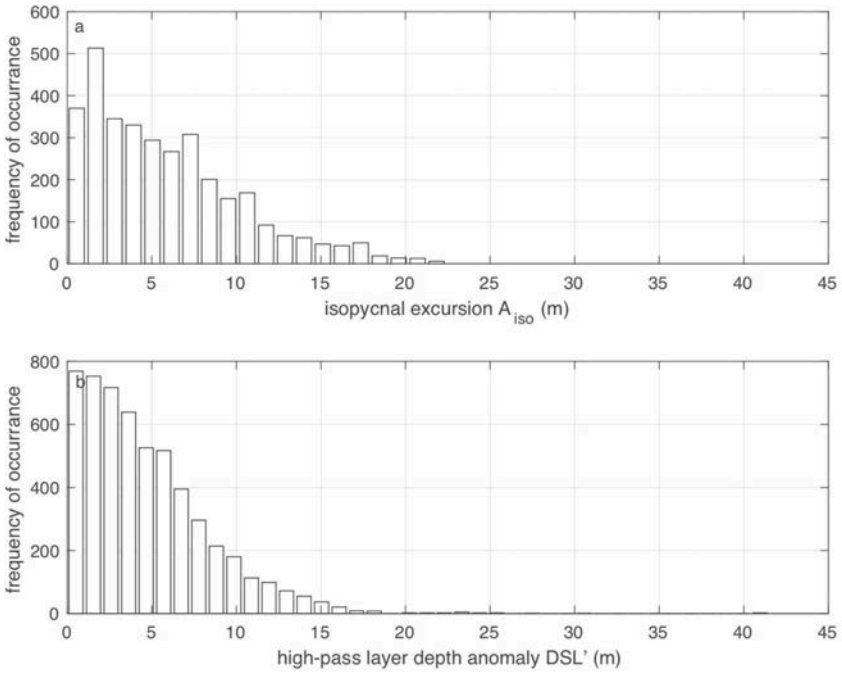

Figure S8: *Histogram of a) the isopycnal excursions of the 26.9 kg m^{-3} potential density contour measured by the Wirewalker (WW), and b) the high-pass layer depth anomalies DSL'.*

Supplementary Materials - References

1. 34. D.A. Siegel, et al. An operational overview of the EXport Processes in the Ocean from RemoTe Sensing (EXPORTS) Northeast Pacific field deployment. Elem Sci Anth, 9: 1. https://doi.org/10.1525/elementa.2020.00107. (2021).

2. T.M. Frank, and E.A. Widder, Effects of a decrease in downwelling irradiance on the daytime vertical distribution patterns of zooplankton and micronekton. *Marine Biology* 140, 1181–1193. https://doi.org/10.1007/s00227-002-0788-7. (2002).

3. M. Stramska, and T.D. Dickey, Short-term variability of the underwater light field in the oligotrohic ocean in response to surface waves and clouds. Deep Sea Research Part I: Oceanographic Research Papers, 45(9) p. 1393-1410, https://doi.org/10.1016/S0967-0637(98)00020-X. (1998).

4. M. Hieronymi, and A. Macke, On the influence of wind and waves on underwater irradiance fluctuations. Ocean Science. 8, p. 455-471. 10.5194/os-8-455-2012. (2012).

5. S. Kaartvedt, A. Røstad, and D.L. Aksnes, Changing weather causes behavioral responses in the lower mesopelagic. Marine Ecology Progress Series, 574: 259–263. (2017).

6. E. Firing, J.M. Hummon, and T.K. Chereskin, Improving the Quality and Accessibility of Current Profile Measurements in the Southern Ocean. Oceanography. 25 https://doi.org/10.5670/oceanog.2012.91. (2012).

7. R.E. Davis, Objective mapping by least squares fitting, J. Geophys. Res., 90(C3), 4773– 4777, doi:10.1029/JC090iC03p04773. (1985).

8. J.H. Cohen, and R.B. Forward, Jr. Zooplankton diel vertical migration—a review of proximate control. Oceanography and Marine Biology, 47: 77–109. (2009).

9. J.H. Cohen, and R.B. Forward, Jr. Diel vertical migration of the marine copepod Calanopia americana. I. Twilight DVM and its relationship to the diel light cycle. Marine Biology 147, 387–398. (2005a).

10. R.B. Forward, Jr. Behavioral responses of larvae of the crab Rhithropanopeus harrisii (Brachyura: Xanthidae) during diel vertical migration. Marine Biology 90, p. 9–18. (1985).

11. J. Ringelberg, Changes in light intensity and diel vertical migration a comparison of marine and freshwater environments. Journal of the Marine Biological Association of the United Kingdom 75, 15-25. (1995).

12. T.M. Frank, and E.A. Widder, The correlation of downwelling irradiance and staggered vertical migration patterns of zooplankton in Wilkinson Basin, Gulf of Maine. Journal of Plankton Research 19, 1975–1991. (1997).

13. J. Ringelberg, and B.J.G. Flik, Increased phototaxis in the field leads to enhanced diel vertical migration. Limnology and Oceanography 39, 1855–1864. (1994)

14. J. Ringelberg, A mechanism of predator-mediated induction of diel vertical migration in Daphnia hyalina. Journal of Plankton Research 13, 83–89. (1991b).

15. J.H. Cohen, and R.B. Forward, Jr. Diel vertical migration in the marine copepod Calanopia americana.
II. The proximate role of exogenous light cues and endogenous rhythms. Marine Biology 147, 399–410. (2005b).

16. J.H. Cohen and R.B. Forward Jr. Photobehavior as an inducible defense in the marine copepod Calanopia americana. Limnology and Oceanography 50(4): 1269-1277. (2005c).

17. R.B. Forward, Jr and W.F. Hettler, Jr. Effects of feeding and predator exposure on photoresponses during diel vertical migration of brine shrimp larvae. Limnology and Oceanography 37, 1261–1270. (1992).

18. J. Ringelberg, The positive phototactic reaction of Daphnia magna Straus: a contribution to the understanding of diurnal vertical migration. Netherlands Journal of Sea Research 2, 319–406. (1964).

19. J. Ringelberg, Enhancement of the phototactic reaction in Daphnia hyalina by a chemical mediated by juvenile perch (Perca fluviatilis). Journal of Plankton Research 13, 17–25. (1991a)

20. J. Ringelberg, Phototaxis as a behavioral component of diel vertical migration in a pelagic Daphnia. Archiv für Hydrobiologie Ergebnisse der Limnologie 39, 45–55. (1993).

21. E. van Gool, and J. Ringelberg, The effect of accelerations in light increase on the phototactic downward swimming

of Daphnia and the relevance to diel vertical migration. Journal of Plankton Research 19, 2041–2050. (1997).

22. N. Daan, and J. Ringelberg, Further studies on the positive and negative phototactic reaction of Daphnia magna Straus. Netherlands Journal of Zoology 19, 525–540. (1969).

23. A.J. Lucas, et al. Adrift Upon a Salinity-Stratified Sea: A View of Upper-Ocean Processes in the Bay of Bengal During the Southwest Monsoon. Oceanography, vol. 29, no. 2, pp. 134–145. (2016).